Monitoring the Effects of the October 10-11 Solar Storm at Mid-Latitudes Using a GNSS SDR Receiver

Monitoring the Effects of the October 10-11 Solar Storm at Mid-Latitudes Using a GNSS SDR Receiver

Iman Ebrahimi Mehr[1], Alex Minetto[1], Emanuele Pica[2], Rayan Imam[2], Claudio Cesaroni[2]
Lucilla Alfonsi[2], Luca Spogli[2,3], Vincenzo Romano[2,3], Fabio Dovis[1]
[1]*Dept. of Electronics and Telecommunications, Politecnico di Torino*, Turin, Italy
[2]*Istituto Nazionale di Geofisica e Vulcanologia (INGV)*, Rome, Italy
[3]*SpacEarth Technology*, Rome, Italy

***Abstract*—The October 10–11, 2024, geomagnetic storm, one of the most intense of solar cycle 25, significantly impacted ionospheric conditions at mid-latitudes. In this study, we analyze the effects of this storm on Global Navigation Satellite System (GNSS) signals using a Software-Defined Radio (SDR)-based receiver at a location in North Italy. The storm, triggered by multiple solar flares and Earth-directed coronal mass ejections (CMEs), induced strong ionospheric disturbances, affecting GNSS signal propagation beyond equatorial and high-latitude regions. To investigate these effects, we recorded GNSS signals on L1 and L2 bands throughout the storm period, along with GNSS observation data from a nearby geodetic station. Our analysis focuses on ionospheric irregularities using the Rate of TEC Index (ROTI) and scintillation indices (S4 and σ_ϕ). ROTI values revealed a significant increase in ionospheric turbulence during the storm's main phase, coinciding with a Kp index of 9 and a Dst minimum of -335 nT. The recorded IQ samples were processed by using a software receiver, showing moderate amplitude scintillation on multiple GNSS satellites. Furthermore, we show the effectiveness of the Software Defined Radio approach, to capture capture and reconstruct ionospheric disturbances with high fidelity for advanced post-processing of the events. The approach is validated by re-playing the recorded GNSS signals and processing the reproduced scenario by means of a commercial GNSS receiver and successfully reproducing scintillation indices.**

***Index Terms*—GNSS; SDR; Ionospheric irregularities; Scintillation; Mid-latitude ionosphere;**

I. Introduction

The ionosphere, a highly dynamic layer of the Earth's upper atmosphere, influences the propagation of radio signals, including those from Global Navigation Satellite Systems (GNSS). On one hand, fluctuations in ionospheric electron density, driven by solar and geomagnetic activity, can introduce signal distortions such as phase and amplitude scintillations. Scintillation impacts GNSS-based Positioning, Navigation, and Timing (PNT) applications by reducing signal quality, causing cycle slips, and degrading positioning accuracy. On the other hand, GNSS signals themselves provide a powerful observational tool for studying ionospheric behavior. As these signals traverse the ionosphere, they carry valuable information about electron density variations, wave-like perturbations, and irregularities that affect signal propagation. By analyzing GNSS data, researchers can monitor ionospheric dynamics, detect space weather disturbances, and assess their impact on satellite-based communication systems. This dual nature—where GNSS signals are both influenced by and serve as probes of the ionosphere—makes them a crucial resource for space weather research.

Traditionally, GNSS-based ionospheric monitoring relied on Ionospheric Scintillation Monitoring Receivers (ISMRs), which provide high-quality measurements of scintillation indices. However, these commercial systems are often closed-source, providing only processed outputs without access to raw signal data that might be valuable source of information for research purposes. In contrast, Software-Defined Radio (SDR) technology not only enables the computation of scintillation indices but also allows for the recording of Intermediate-Frequency (IF) and In-phase/Quadrature (IQ) signals, which serve as the foundation for these indices. This approach has been successfully employed in past investigations, [1]–[7] and it has been the basis for the analysis presented in this paper.

Disturbances in GNSS signals caused by ionospheric irregularities, such as scintillation, are more commonly observed in equatorial and high-latitude regions. However, under strong geomagnetic storms conditions, like the Mother's Day storm in May 2024 [8] and the recent geomagnetic storm of October 10–11, 2024 [9]–[11], also mid-latitude regions can experience significant ionospheric disturbances, necessitating dedicated investigations for the latter regions. Geomagnetic storms, driven by solar flares and Coronal Mass Ejections (CMEs), inject large amounts of energy into the Earth's magnetosphere, triggering ionospheric irregularities that can extend beyond their typical occurrence zones. In particular, the October 2024 geomagnetic storm was one of the most intense of solar cycle 25, causing global disturbances in the ionosphere, including mid-latitude effects. This storm, associated with multiple solar flares and Earth-directed CMEs, provided a unique opportunity to study the extension of ionospheric irregularities beyond equatorial and polar regions, affecting GNSS signal propagation at unusual latitudes.

During this period, we leveraged an SDR-based approach using the Navigation Signal Monitoring, Analysis, and Record-

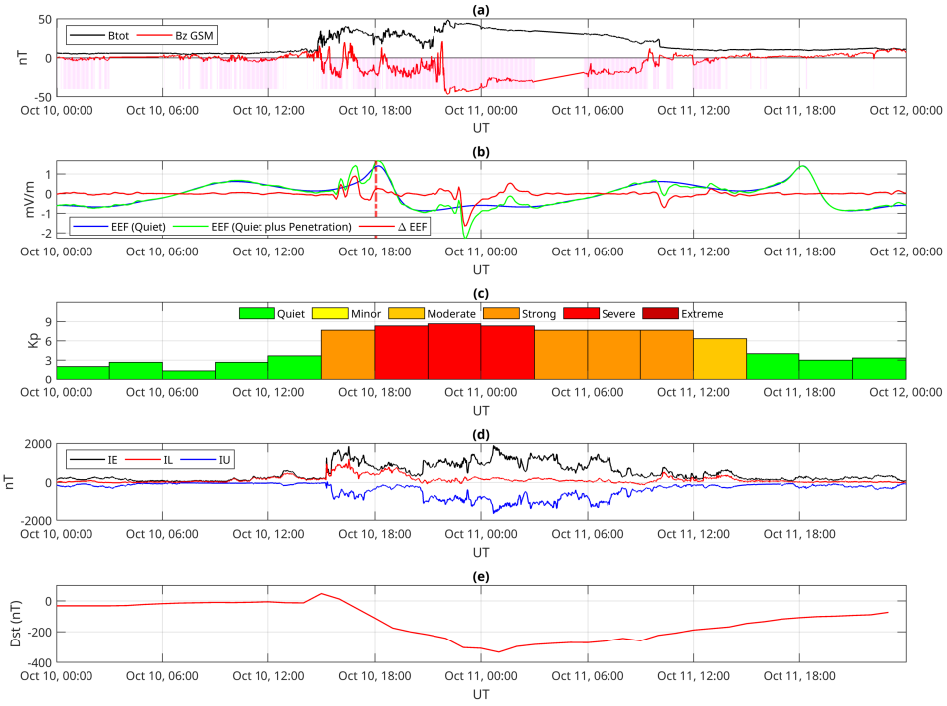

Fig. 1: Time profiles for 10-11 October 2024 of: (a) IMF Btot (black) and Bz in GSM coordinates (red); (b) quiet EEF (blue), quiet plus penetration EEF (green) and the delta value between the two (red) in the longitudinal sector under observation; the red dashed line indicates the sunset time at the magnetic equator in the longitudinal sector of the observations; (c) Kp index and related intensity of the geomagnetic storm according to NOAA scale (various colours); (d) IE (black), IL (red) and IU (blue) auroral index; (e) Dst index. Credits

ing Tool (N-SMART) [12], [13] to record and analyze GNSS signals. This platform enabled the collection of IQ signal samples, allowing for a detailed spectral and scintillation analysis of GNSS data during the storm event. The IQ signal samples of GNSS signals in L1 and L2 bands were recorded in Turin, Italy (45.0703° N, 7.6869° E), providing valuable data for analyzing the effects of this storm on GNSS signal propagation at mid-latitudes.

II. BACKGROUND

A. Ionospheric Scintillation at Middle-Latitude

Ionospheric scintillation refers to rapid fluctuations in the amplitude and phase of radio signals as they traverse irregularities in the Earth's ionosphere. While traditionally associated with equatorial and high-latitude regions, recent studies have highlighted the occurrence and significance of scintillation phenomena at mid-latitudes [14]. At mid-latitudes, scintillation events are generally less frequent and less intense compared to equatorial and polar regions. However, during periods of heightened solar and geomagnetic activity, such as geomagnetic storms, the mid-latitude ionosphere can exhibit significant irregularities. These disturbances can lead to notable scintillation effects, impacting the reliability of satellite-based communication and navigation systems [8]. The primary drivers of mid-latitude scintillation include geomagnetic storms, traveling ionospheric disturbances (TIDs) and equatorial plasma bubbles (EPBs). Geomagnetic storms, driven by solar flares and coronal mass ejections (CMEs), inject large amounts of energy into the Earth's magnetosphere, triggering ionospheric irregularities that can extend beyond their typical occurrence zones [15]. TIDs are wave-like perturbations in the ionosphere's electron density, often originating from atmospheric gravity waves. TIDs can modulate ionospheric conditions, contributing to scintillation effects at mid-latitudes [16], [17]. Additionally, severe L-band scintillation over low-to-mid latitudes can be caused by Extreme Equatorial Plasma Bubbles (EPBs), as reported by several studies [18]–[22]. Under certain conditions, EPBs can expand poleward, leading to significant signal degradation in GNSS receivers at mid-latitudes, further emphasizing the need for continuous monitoring and research into these disturbances.

B. The October 2024 Geomagnetic Storm and Its Effects

On 10 October 2024 was observed the second most important storm of the ongoing solar cycle 25. The storm was associated with a X2.1 flare on 7 October and a X1.8 solar flare on 9 October giving rise to a chain of CMEs impacting the Earth's magnetosphere on 10 October. The CMEs induced a geomagnetic storm at planetary level with a Dst [23] peak of

-335 nT on 11 October 2024 (Fig. 1(e)) and a maximum Kp value [24] of 8+ at 21 UT of 10 October (Fig. 1(c)). The related shock was recorded in the Interplanetary Magnetic Field (IMF) Btot (black) and Bz (red) parameters [25] reported in Fig. 1(a). The sudden increase of southward Bz conditions at the arrival of the shock in the afternoon of 10 October (Fig. 1(a)) caused an intensification in the IE, IL and IU auroral electrojet indices [26] in the European high-latitude sector (Fig. 1(d)) which may cause Disturbance Dynamo Electric Fields (DDEFs) possibly impacting the low latitude electrodynamics. Fig. 1(b) reports the Equatorial Electric Field (EEF) model from Cooperative Institute for Research in Environmental Sciences (CIRES) of the University of Boulder, showing an intensification of the EEF due to Prompt Penetrating Electric Fields (PPEFs) [27] right before the sunset time (red dashed line of Fig. 1(a)) at the magnetic equator in the longitudinal sector under observation on 10 October, which also corresponds to the peak of the EEF featuring the Pre-revesal Enhancement (PRE). The interplay between PPEFs and DDEFs [28]–[31] possibly generates a super-fountain-like effect with a poleward extension of Equatorial Plasma Bubbles (EPBs) impacting the GNSS signals up to mid-latitudes during the storm. The storm generates visible aurora-like phenomena which might be linked to Stable Auroral Red (SAR) arcs [8] at mid-latitudes like in the Turin area as reported in Fig.2.

Fig. 2: Aurora Photo taken at 20:55 UTC from Turin. Credits F. Dovis.

III. METHODOLOGY

The methodology presented in this study is based on an optimized version of an SDR-based GNSS ionospheric monitoring system, originally developed as part of the DemoGRAPE project in 2015. This earlier version was a prototype SDR architecture, installed at the South African Antarctic base SANAE IV. The project was an international collaboration funded by the Italian National Program for Antarctic Research (PNRA) and led by the Istituto Nazionale di Geofisica e Vulcanologia (INGV), in partnership with Politecnico di Torino, the South African National Space Agency (SANSA), and the Brazilian National Institute of Space Physics.

The DemoGRAPE SDR system was designed to work in parallel with a commercial Ionospheric Scintillation Monitoring Receiver (ISMR)—a Septentrio PolaRxS receiver—sharing the same antenna. Since its installation in 2015, both systems have been continuously monitoring the ionosphere, enabling comparisons between traditional commercial GNSS monitoring systems and SDR-based solutions [32].

A. Hardware Configuration of the Monitoring Station

Building upon the knowledge and experience gained from DemoGRAPE, the Navigation Signal Analysis and Simulation (NavSAS) group at Politecnico di Torino developed an advanced GNSS SDR monitoring platform, named the Navigation Signal Monitoring, Analysis, and Recording Tool (N-SMART) [12]. The monitoring station is designed to capture GNSS signals at IF frequency for scintillation monitoring and ionospheric studies. It consists of several interconnected components that ensure precise and reliable data acquisition. The complete hardware architecture is illustrated in Fig. 3. A detailed description of each hardware component is provided below:

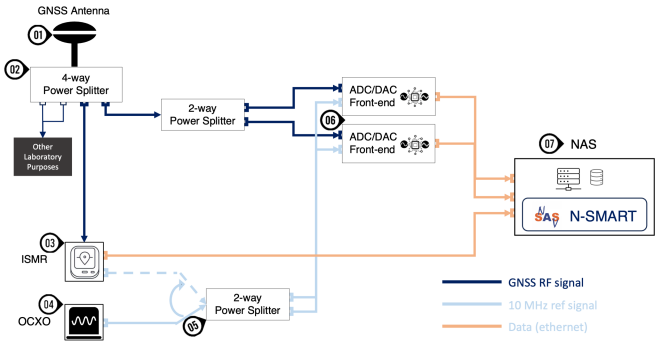

Fig. 3: Hardware scheme.

1) **GNSS Antenna:** The antenna is a reference 3D choke ring ground plane that supports multiple GNSS constellations and bands with remarkable multipath rejection performance. It incorporates a built-in Low-Noise-Amplifier (LNA) with a gain of 29 dB.
2) **4-Way Splitter:** This is an active power splitter that distributes the received GNSS signals to four RF outputs, with each output additionally amplified by 10 dB. The antenna is connected to this splitter through a 60 m low-attenuation coaxial cable.
3) **Ionospheric Scintillation Monitoring Receiver (ISMR):** The ISMR used in this project is the Septentrio PolaRx5s, a multi-band, multi-frequency GNSS receiver designed for high-precision ionospheric and scintillation monitoring. Its capability to record dual-frequency signals from all major GNSS constellations makes it suitable for measuring Total Electron Content (TEC) and detecting ionospheric irregularities, including amplitude and phase scintillations.
4) **OCXO:** This refers to an oven-controlled crystal oscillator, which serves as a highly reliable and stable

$10\,\mathrm{MHz}$ clock source for front-end devices. An external clock is essential for SDR-based front-end systems to provide stable and accurate frequency references, ensuring precise timing for signal sampling and processing. Additionally, as a backup solution in this architecture, it is possible to use the reference clock output from the Septentrio receiver, which provides the same $10,\mathrm{MHz}$ output but at a lower voltage of 1.1 V compared to the 3.3 V of the OCXO. To assess the effects of these two signals as reference clocks, two simultaneous 20-minute signal captures were performed at the L1/E1 center frequency using two separate USRPs: one disciplined by an external OCXO and the other disciplined by the REF_OUT signal of a Septentrio PolaRx5S receiver. The comparison analyzed the outputs of the phase-locked loop (PLL) and delay-locked loop (DLL) using a signal sampled at $10,\mathrm{MHz}$ with 8-bit quantization. The results demonstrate that the PLL and DLL discriminator outputs are comparable between the two configurations, with the OCXO exhibiting slightly lower variance.

5) **2-Way Power Splitters:** A 2-way coaxial power splitter/combiner (Mini-Circuits ZMSC-2-1W+) with a wideband range of 1 to $650\,\mathrm{MHz}$ MHz is used to distribute the $10\,\mathrm{MHz}$ output signal from the OCXO to the two front-end devices. Another 2-way splitter (Mini-CircuitZAPD-2-s+), with a bandwidth of 1 to 2 GHz, is used to split GNSS signals.
6) **ADC/DAC Front-End:** The front-end devices are Ettus Research Universal Software Radio Peripheral (USRP) N210 units. These devices perform analog-to-digital conversion of the RF input signal and record IF signal samples into binary (`.bin`) files.
7) **NAS:** A Network Attached Storage (NAS) system serves as a centralized data storage solution, hosting the N-SMART platform in a containerized environment. This platform functions as the core application for storing the large volume of digital samples of GNSS signals generated by the front-ends, managing and processing recorded data.

B. Software Architecture for Signal Processing

N-SMART is a modular and open software architecture tailored for GNSS signal monitoring, analysis, and high-fidelity recording. It efficiently addresses previous challenges such as data transfer bottlenecks and scalability issues by leveraging containerized software using Docker container. This container encapsulates all necessary software components, for RF front-end communication, signal acquisition and processing, user interface (UI) for monitoring, configuring station and in-field analysis [12].

This flexible architecture has been further extended in this work to enhance its capability for GNSS signal scintillation monitoring. The following sections detail the newly introduced features aimed at handling recorded signals for this specialized application. N-SMART, as its main task, continuously records signals based on the configured settings (detailed in section III-C) and generates IQ samples of the recorded signal. After the signal grabbing is complete, the post-processing of the IQ signal samples begins, which involves three steps as follows:

1) Processing Data with the GNSS Software Receiver: This component processes raw data collected by the station. The registered signal is first down-sampled from 10 MHz to 5 MHz to meet the requirements of the receiver, and 1-bit quantization is applied to the signal sample to ensure compatibility. The resulting output comprises in-phase and quadrature components of the prompt correlator and phase measurements from the tracking loop for each PRN, limited to the GPS constellation, with an integration time of 20 ms. Note that this converted file is temporary and will be deleted upon process completion, while the original file is preserved.
2) Calculation of Scintillation Indexes: Scintillation indexes are calculated from the receiver's output over a 1-minute window, aligning with the window duration used by the Septentrio receiver for comparison. Additionally, the azimuth and elevation of each satellite are calculated using the navigation message demodulated from the tracking loop output. The results are stored in a dedicated database table for subsequent analysis and decision-making.
3) Decision-Making for File Management: A decision-making strategy evaluates the recorded data to determine whether files should be retained or deleted based on the detection of scintillation events. For instance, files may be retained if the S4 index exceeds a threshold of 0.25 in more than (equal) 5 instances within the defined chunk. These thresholds and limits for this process can be configured via the N-SMART interface. The strategy can operate in three modes:
   - Using data from both the software and Septentrio receivers.
   - Using data solely from the software receiver.
   - Using data solely from the Septentrio receiver.

Additionally, in order to collect data from the Septentrio receiver, a virtual machine environment with Ubuntu OS has been deployed on the NAS. This virtual machine has access to a dedicated shared folder through the Network File System (NFS) protocol on the NAS to log data in 15-minute windows. These logs include Septentrio binary files (`.sbf`), generated scintillation indexes (`.ismr`), GNSS raw observation files (RINEX) and navigation messages. N-SMART also has access to the same folder to read `.ismr` files and insert them into the database for the decision-making task.

C. Dataset collection

1) IQ Dataset: During the geomagnetic storm of October 10–11, IQ samples of GNSS signals were collected at the NavSAS laboratory, Turin, Italy (geodetic coordinates of the antenna: Latitude 45° 03' 51.8968" N, Longitude 7° 39' 43.0717" E, Altitude: 322.3106 m). The measurements were obtained using the hardware configuration detailed in Section

III-A. The experimental setup utilized two USRPs disciplined with an external OCXO; one was configured to acquire GNSS L1 signals at 1.57542 GHz, while the other captured L2 signals at 1.2276 GHz. Both front-ends recorded signals at a sampling frequency of 10 MHz with 8-bit quantization. The data collection spanned 14:30 UTC on October 10 to 21:30 UTC on October 11, encompassing the peak and recovery phases of the solar storm. The window for each IQ file registration was set to 50 minutes (approximately 56 GB), with a half-second interval between consecutive windows.

2) Scintillation Indexes Dataset: For the mentioned period of the solar storm, two sets of scintillation indexes were extracted: one from the SDR receiver and the other from the Septentrio receiver. The first set was obtained using the procedure detailed in Section III-B and stored in the database as well as in `.ismr` files. During that period, the Septentrio receiver was not included in the architecture described earlier. Instead, the scintillation indexes were extracted using a record-and-replay paradigm (post-processing). In this process, the recorded IQ signals was replayed through a USRP configured to match the original recording setup. The replayed signal was fed into the Septentrio receiver, which was able to track only GPS and Galileo satellite signals. The scintillation indexes were then calculated directly by the Septentrio receiver's internal algorithms. The computed indexes were subsequently logged and archived for comparison with those extracted from the SDR-based processing.

3) Rinex Observation Dataset: The rinex observation dataset is available from the geodetic GNSS station TORI00ITA, located 129.25 meters away from the antenna used for the IQ dataset generation and part of the EUREF Permanent GNSS Network (https://www.epncb.oma.be/). This station provides multi-constellation rinex observation data, including GPS, Galileo, GLONASS, and BeiDou signals. The available data from this station were utilized to compute the Rate of TEC Index using the L1 and L2 GNSS obervables sampled at 30s in order to characterize the temporal and spatial variations of medium-scale ionospheric irregularities.

D. Description of Scintillation Parameters

This section describes the key parameters used for analyzing ionospheric scintillations in GNSS signals: the amplitude scintillation index (S_4), the phase scintillation index (σ_ϕ), and the rate of total electron content index (ROTI). These parameters quantify the effects of ionospheric irregularities on GNSS signals, which are critical for evaluating the impact of scintillation on satellite-based communication and navigation systems. Together, S_4, σ_ϕ, and ROTI provide a robust framework for assessing ionospheric scintillation effects on GNSS signals. While S_4 and σ_ϕ focus on small-scale irregularities causing amplitude and phase disturbances, ROTI captures larger-scale TEC gradients, making these indices essential for monitoring and mitigating the impact of scintillation on satellite communication systems [8].

1) Rate of Total Electron Content Index (ROTI): The ROTI index evaluates the temporal rate of change of the total electron content (TEC) along the GNSS signal path. It is derived from the rate of TEC change ($\Delta TEC/\Delta t$) and serves as an indicator of medium- to large-scale irregularities [33] [34].

$$ROTI = \sqrt{\langle \left(\frac{dTEC}{dt}\right)^2 \rangle - \langle \frac{dTEC}{dt} \rangle^2} \tag{1}$$

where dTEC can be calculted as:

$$\frac{dTEC}{dt} = \frac{VTEC_{i+1} - VTEC_i}{t_{i+1} - t_i} \tag{2}$$

Here $STEC_i$ and $STEC_{i+1}$ are the slant TEC values at two consecutive time points t_i and t_{i+1}. The STEC from from dual-frequency GNSS measurements, can be derived using:

$$STEC = \frac{f_1^2 f_2^2}{40.3(f_1^2 - f_2^2)} \times [P_1 - P_2] \tag{3}$$

where:

- f_1 and f_2 are the frequencies of the two GNSS signals (e.g., L1 and L2).
- P_1 and P_2 are the pseudoranges measured on the two frequencies.
- The constant 40.3 converts the result into TEC units (TECU, where 1 TECU $= 10^{16}$ electrons/m^2).

While STEC represents the total electron content along the slanted path between the satellite and the receiver, it is essential to convert it to Vertical TEC (VTEC) to standardize measurements and account for variations due to satellite geometry. This conversion ensures that the derived ROTI reflects ionospheric irregularities independent of the satellite's elevation angle, providing a more consistent and comparable metric. The STEC can be converted to VTEC using the following formula:

$$VTEC = STEC \times \cos(z) \tag{4}$$

where:

- z is the zenith angle of the GNSS signal, which can be computed as $z = \arcsin(\sin(e)/R)$, where e is the satellite elevation angle, and R accounts for Earth curvature and ionospheric height.
- $\cos(z)$ is the obliquity factor that adjusts STEC to VTEC.

Using this computed VTEC, the time derivative $\frac{dTEC}{dt}$ can be obtained as follows:

IV. Results and discussion

A. ROTI Variability and Detection of Ionospheric Disturbances

The ROTI has been computed over 5-minute intervals from the TORI00ITA geodetic receiver in order to detect possible time-windows of disturbed ionospheric conditions affecting the GNSS signals propagation. An elevation mask of 30° has been applied to filter out low-elevation signals, reducing multipath and measurement noise. Fig.4 presents

ROTI values over four consecutive days, providing insight into the temporal evolution of possible ionospheric disturbances. In Fig.4, different colors of the ROTI values accounts for different satellites in the field-of-view. Throughout most of the observation period, ROTI values remain relatively low, indicating stable TEC conditions. However, a notable increase in ROTI is observed between 18:00 and midnight on October 10, 2024, suggesting a significant enhancement of ionospheric irregularities during this timeframe. This period of intensified ionospheric activity correlates strongly with the geomagnetic storm, as indicated by the Kp index reaching approximately 9 during the same timeframe (as shown in Fig. 1 (c)). A Kp value of 9 corresponds to a severe geomagnetic storm, which can lead to increased ionospheric turbulence, affecting the propagation of GNSS signals. Moreover, in Fig.4 the vertical red dashed line report the sunset time at the magnetic equator in the longitudinal sector under observation, highlighting that most of the high ROTI values are observed during the post-sunset hour of the 10 October. This is consistent with the presence of EPBs migrating poleward and reaching the field-of-view of the GNSS receiver. Indeed, as reported in 1 (b), the storm-induced intensification of the EEF right before the sunset time possibly generates a super-fountain-like effect at the magnetic equator.

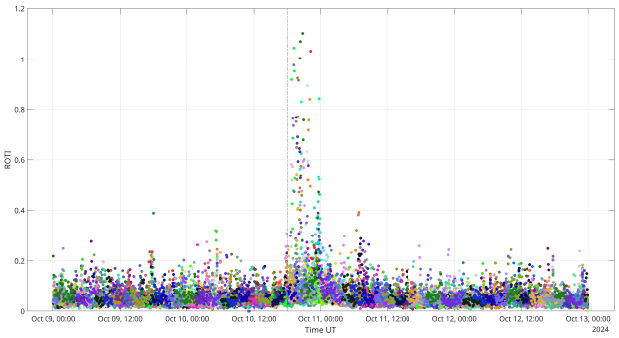

Fig. 4: ROTI from TORI00ITA receiver from 9/10 to 12/10, elevation mask 30°. Different colors accounts for different satellites. The vertical red dashed line indicates the sunset time at the magnetic equator in the longitudinal sector of the observations.

B. processing the IQ samples with Software receiver

Considering the time-vindow identified by the ROTI values, the results presented in this section are derived from processing the recorded IQ files (explained in Section III-C) and analyzed using a software receiver that extracts ionospheric scintillation parameters, including the S4 index and σ_ϕ. Figure 5 shows the S4 index from the different satellites in view during October 10 and 11 in the interval 18:00 to 22:15 UT and applying an elevation mask of 30 degrees. On October 10, the S4 index exhibits moderate scintillation values ($S4 > 0.1$) on different GPS satellites. This coincide with the main phase of the storm, with a Kp index of approximately 9, and they are possibly

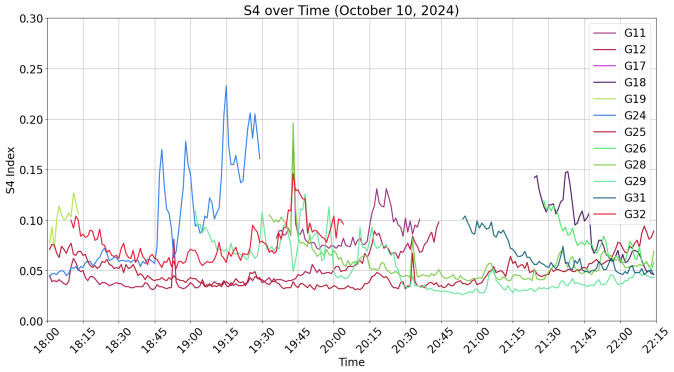

(a) October 10, 2024

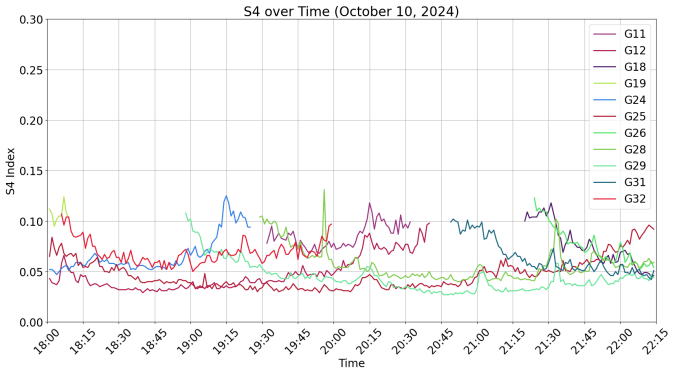

(b) October 11, 2024

Fig. 5: S4 Index Variations on October 10 and 11, 2024.

related to ionospheric irregularities embedded in EPBs migrating northward while moving along the magnetic lines, as already previously mentioned. On the contrary, on October 11, no S4 index values above weak scintillation ($S4 > 0.1$) are detectable, suggesting no detectable ionospheric irregularities capable to affect the GNSS signal propagation at mid-latitudes. Indeed, as it is possible to see from Fig. 1, the geomagnetic condition on 11 October were quieter compared to the 10 and no clear enhancement on the EEF causing super-fountain-like effect are detectable.

C. Analysis of Scintillation on Low-Elevation Satellite G32

The analysis of satellite G32, which was observed at a low elevation angle of 15 degrees, provides insights into ionospheric scintillation effects. To ensure that the observed fluctuations are not attributed to multipath effects, data from two consecutive days, October 10 and 11, 2024, were analyzed. Despite the low elevation angle, which could potentially introduce multipath interference, the antenna used in this study is multipath-resilient, and the surrounding environment offers an open-sky view, minimizing the likelihood of signal reflections.

The S4 and σ_ϕ indices were extracted from the recorded IQ files using two different processing methods: a software receiver (SRX) and the ISMR receiver through replayed IQ

data. The results, presented in Figure 6, show that on October 10, both S4 and σ_ϕ indices exceed the typical threshold values, indicating that satellite G32 experienced real scintillation effects rather than multipath interference. This observation aligns with the high geomagnetic activity on October 10 and with the ionospheric disturbed condition reported by the ROTI in Fig. 4. The agreement between the software receiver (SRX) and ISMR receiver results further supports the reliability of the extracted indices. While small variations between the two processing methods are present, the overall trends remain consistent, reinforcing the validity of the detected scintillation.

V. Conclusion

This study shows first results of analyzing the impact of the October 10–11, 2024, geomagnetic storm on GNSS signal propagation at mid-latitudes using an SDR-based receiver in Turin, Italy. By recording GNSS signals on L1 and L2 bands and processing them with a software receiver, we assessed the ionospheric irregularities through the S4 and σ_ϕ scintillation indices. Additionally, GNSS observations from a nearby geodetic station allowed us to compute the Rate of TEC Index (ROTI), which revealed increased ionospheric turbulence during the storm's main phase, coinciding with a peak Kp index of 9 and a Dst minimum of -335 nT.

The results confirmed the presence of moderate amplitude scintillation on multiple GNSS satellites, aligning with the expected disturbances caused by the geomagnetic storm. The analysis also identified enhanced ROTI values during the post-sunset hours, suggesting the presence of equatorial plasma bubble (EPB) extensions reaching mid-latitudes. Furthermore, we replayed the recorded GNSS signals through a Septentrio receiver and successfully reproduced scintillation indices, demonstrating that the setup was able to effectively capture and reconstruct ionospheric disturbances. This highlights the importance of SDR-based data collection, as it enables detailed post-event analysis and the validation of different processing techniques.

Future work will focus on further analysis of the recorded GNSS signals on both L1 and L2 bands, extending the study to additional GNSS constellations beyond GPS. This will provide a more comprehensive understanding of ionospheric disturbances across different satellite systems and enhance the robustness of space weather monitoring at mid-latitudes. The ability to store and replay IQ data for post-processing opens new opportunities for refining scintillation detection methods and improving real-time GNSS monitoring strategies.

ACKNOWLEDGMENT

The Ph.D. work of I. Ebrahimi Mehr is supported by the grant DOT1332092 CUP E11B21006430005 funded within the Italian Programma Operativo Nazionale (PON) Ricerca e Innovazione 2014-2020, Asse IV "Istruzione e ricerca per il recupero" con riferimento all'Azione IV.4 "Dottorati e contratti di ricerca su tematiche dell'innovazione" e all'Azione IV.5 "Dottorati su tematiche green" DM 1061/2021. Rayan Imam's current research fellowship is funded by the Swarm Space Weather Variability, Irregularities, and Predictive Capabilities for the Dynamic Ionosphere (Swarm-VIP-Dynamic) project, which has been funded by the European Space Agency, contract 4000143413/23/I-EB within the "ESA Solid Magnetic Science Cluster - Research Opportunities: 4dionosphere - Expro+".

References

[1] N. Linty, F. Dovis, and L. Alfonsi, "Software-defined radio technology for GNSS scintillation analysis: bring antarctica to the lab," *GPS Solutions*, vol. 22, 07 2018.

[2] R. Imam, L. Alfonsi, L. Spogli, C. Cesaroni, I. Ebrahimi Mehr, A. Minetto, and F. Dovis, "Scintillation climatology from a software defined radio receiver over antarctica," *Annals of Geophysics*, vol. 67, p. PA108, 05 2024.

[3] E. Pica, A. Minetto, C. Cesaroni, and F. Dovis, "Analysis and characterization of an unclassified RFI affecting ionospheric amplitude scintillation index over the mediterranean area," *IEEE Journal of Selected Topics in Applied Earth Observations and Remote Sensing*, vol. 16, pp. 8230–8248, 2023.

[4] C. Cristodaro, F. Dovis, N. Linty, and R. Romero, "Design of a configurable monitoring station for scintillations by means of a GNSS software radio receiver," *IEEE Geoscience and Remote Sensing Letters*, vol. 15, no. 3, pp. 325–329, 2018.

[5] C. Cristodaro, L. Ruotsalainen, and F. Dovis, "Benefits and limitations of the record and replay approach for GNSS receiver performance assessment in harsh scenarios," *Sensors*, vol. 18, no. 7, 2018. [Online]. Available: https://www.mdpi.com/1424-8220/18/7/2189

[6] N. Linty, F. Dovis, R. Romero, C. Cristodaro, L. Alfonsi, and E. Correia, "Monitoring ionosphere over antarctica by means of a GNSS signal acquisition system and a software radio receiver," in *Proceedings of the 2016 International Technical Meeting of The Institute of Navigation, Monterey, California,*, 02 2016, pp. 549–555.

[7] R. Imam, L. Alfonsi, L. Spogli, C. Cesaroni, and F. Dovis, "On estimating the phase scintillation index using TEC provided by ISM and IGS professional GNSS receivers and machine learning," *Advances in Space Research*, vol. 73, no. 7, pp. 3753–3771, 2024, recent advances in equatorial, low- and mid-latitude mesosphere, thermosphere and ionosphere studies. [Online]. Available: https://www.sciencedirect.com/science/article/pii/S0273117723005744

[8] L. Spogli, T. Alberti, P. Bagiacchi, l. cafarella, C. Cesaroni, G. Cianchini, I. Coco, D. Di Mauro, r. ghidoni, F. Giannattasio, A. Ippolito, c. marcocci, M. Pezzopane, E. Pica, A. Pignalberi, L. Perrone, V. Romano, D. Sabbagh, C. Scotto, and m. viola, "The effects of the may 2024 mother's day superstorm over the mediterranean sector: from data to public communication," *Annals of geophysics = Annali di geofisica*, vol. 67, p. 218, 06 2024.

[9] V. Pierrard, N. Bergeot, T. Verhulst, and J. Chevalier, "Effects of the geomagnetic superstorms of 10–11 may 2024 and 7–11 october 2024 on the ionosphere and plasmasphere," *Preprints*, 2025. [Online]. Available: https://www.preprints.org/frontend/manuscript/44bccca9b5dacadb7d3fefa0c4c4c8c9/download_pub

[10] D. Oliveira, E. Zesta, and D. Nandy, "The 10 october 2024 geomagnetic storm may have caused the premature reentry of a starlink satellite," *Frontiers in Astronomy and Space Sciences*, 2025. [Online]. Available: https://www.frontiersin.org/journals/astronomy-and-space-sciences/articles/10.3389/fspas.2024.1522139/full

[11] G. da Silva Picanço, P. Fagundes, and J. Moro, "Dynamics of polar-equatorial ionospheric irregularities during the 10-13 october 2024 superstorm," *ESS Open Archive*, 2024. [Online]. Available: https://essopenarchive.org/doi/pdf/10.22541/essoar.173462761.19206822

[12] I. E. Mehr, A. Minetto, F. Dovis, E. Pica, C. Cesaroni, and V. Romano, "An open architecture for signal monitoring and recording based on SDR and docker containers: A GNSS use case," in *IEEE EUROCON 2023 - 20th International Conference on Smart Technologies*, 2023, pp. 66–71.

[13] I. E. Mehr, A. Minetto, and F. Dovis, "A navigation signals monitoring, analysis and recording tool: Application to real-time interference detection and classification," in *Proceedings of the 36th International Technical Meeting of the Satellite Division of The Institute of Navigation (ION GNSS+ 2023)*. Institute of Navigation, oct 2023. [Online]. Available: https://doi.org/10.33012%2F2023.19391

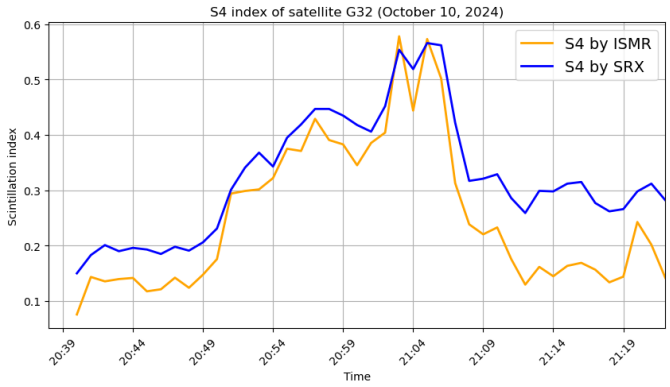

(a) S4 index, October 10, 2024

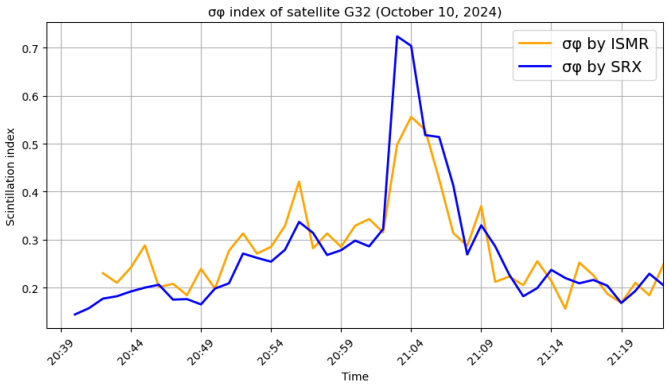

(b) σ_ϕ index (rad), October 10, 2024

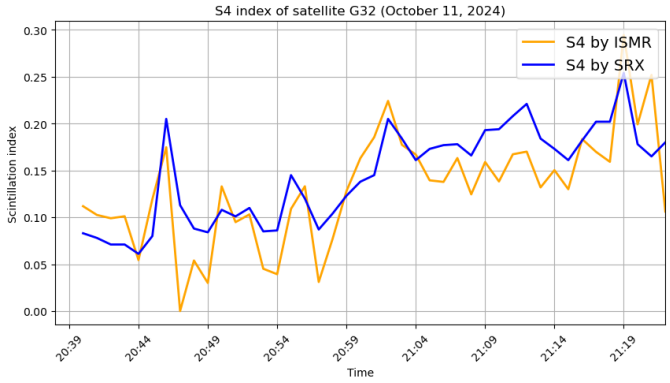

(c) S4 index, October 11, 2024

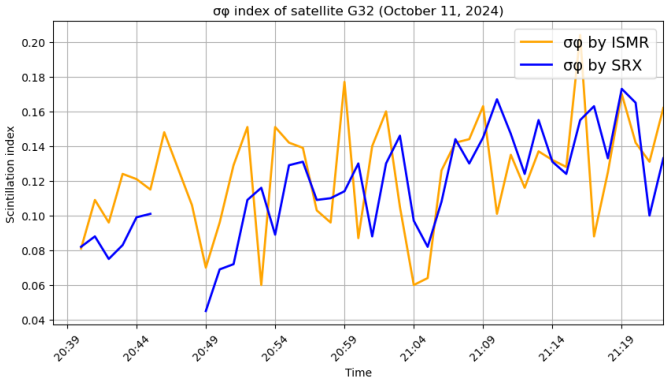

(d) σ_ϕ index (rad), October 11, 2024

Fig. 6: Satellite G32 indices for October 10 and 11, 2024.

[14] I. Gulati, H. Li, S. Stainton, M. Johnston, and S. Dlay, "Investigation of ionospheric phase scintillation at middle-latitude receiver station," in *2019 International Symposium ELMAR*, 2019, pp. 191–194.

[15] C. I. Uga, S. P. Gautam, and E. B. Seba, "TEC disturbances caused by CME-triggered geomagnetic storm of september 6–9, 2017," *Heliyon*, vol. 10, no. 10, p. e30725, 2024. [Online]. Available: https://www.sciencedirect.com/science/article/pii/S2405844024067562

[16] G. M. Smith and A. B. Kebede, "Investigation of traveling ionospheric disturbances during a midlatitude spread F event," *arXiv: Space Physics*, 2010. [Online]. Available: https://api.semanticscholar.org/CorpusID:119220570

[17] Fallows, Richard A., Forte, Biagio, Astin, Ivan, Allbrook, Tom, Arnold, Alex, Wood, Alan, Dorrian, Gareth, Mevius, Maaijke, Rothkaehl, Hanna, Matyjasiak, Barbara, Krankowski, Andrzej, Anderson, James M., Asgekar, Ashish, Avruch, I. Max, Bentum, Mark, Bisi, Mario M., Butcher, Harvey R., Ciardi, Benedetta, Dabrowski, Bartosz, Damstra, Sieds, de Gasperin, Francesco, Duscha, Sven, Eislöffel, Jochen, Franzen, Thomas M.O., Garrett, Michael A., Grießmeier, Jean-Matthias, Gunst, André W., Hoeft, Matthias, Hörandel, Jörg R., Iacobelli, Marco, Intema, Huib T., Koopmans, Leon V.E., Maat, Peter, Mann, Gottfried, Nelles, Anna, Paas, Harm, Pandey, Vishambhar N., Reich, Wolfgang, Rowlinson, Antonia, Ruiter, Mark, Schwarz, Dominik J., Serylak, Maciej, Shulevski, Aleksander, Smirnov, Oleg M., Soida, Marian, Steinmetz, Matthias, Thoudam, Satyendra, Toribio, M. Carmen, van Ardenne, Arnold, van Bemmel, Ilse M., van der Wiel, Matthijs H.D., van Haarlem, Michiel P., Vermeulen, René C., Vocks, Christian, Wijers, Ralph A.M.J., Wucknitz, Olaf, Zarka, Philippe, and Zucca, Pietro, "A lofar observation of ionospheric scintillation from two simultaneous travelling ionospheric disturbances," *J. Space Weather Space Clim.*, vol. 10, p. 10, 2020. [Online]. Available: https://doi.org/10.1051/swsc/2020010

[18] J. Sousasantos, J. G. Socola, F. S. Rodrigues, R. W. Eastes, C. G. M. Brum, and P. Terra, "Severe L-band scintillation over low-to-mid latitudes caused by an extreme equatorial plasma bubble: joint observations from ground-based monitors and GOLD," *Earth, Planets and Space*, vol. 75, pp. 1–12, 2023. [Online]. Available: https://api.semanticscholar.org/CorpusID:257634086

[19] E. Pica, L. Spogli, C. Cesaroni, L. Alfonsi, H. Haralambous, F. Vallianatos, G. De Franceschi, V. Romano, and C. Marcocci, "Assessing the ionospheric scintillations occurrence on L-band in the Southern Mediterranean sector," *Advances in Space Research*, vol. 75, no. 1, pp. 837–855, 2025. [Online]. Available: https://www.sciencedirect.com/science/article/pii/S0273117724010597

[20] I. Cherniak and I. Zakharenkova, "First observations of super plasma bubbles in Europe," *Geophysical Research Letters*, vol. 43, no. 21, pp. 11,137–11,145, 2016. [Online]. Available: https://agupubs.onlinelibrary.wiley.com/doi/abs/10.1002/2016GL071421

[21] D. K. Karan, C. R. Martinis, R. W. Eastes, R. E. Daniell, W. E. McClintock, and C.-S. Huang, "GOLD observations of equatorial plasma bubbles reaching mid-latitudes during the 23 April 2023 geomagnetic storm," *Space Weather*, vol. 22, no. 6, p. e2023SW003847, 2024, e2023SW003847 2023SW003847. [Online]. Available: https://agupubs.onlinelibrary.wiley.com/doi/abs/10.1029/2023SW003847

[22] A. Morozova, L. Spogli, T. Barata, R. Imam, E. Pica, J. A. Cahuasquí, M. M. Hoque, N. Jakowski, and D. Estaço, "Scintillations in Southern Europe during the geomagnetic storm of June 2015: analysis of a plasma bubbles spill-over using ground-based data," 2024. [Online]. Available: https://arxiv.org/abs/2412.06608

[23] K. World Data Center for Geomagnetism, M. Nose, T. Iyemori, M. Sugiura, and T. Kamei, "Geomagnetic Dst index," 2015. [Online].

Available: https://doi.org/10.17593/14515-74000
[24] J. Matzka, C. Stolle, Y. Yamazaki, O. Bronkalla, and A. Morschhauser, "The geomagnetic Kp index and derived indices of geomagnetic activity," *Space Weather*, vol. 19, no. 5, p. e2020SW002641, 2021, e2020SW002641 2020SW002641. [Online]. Available: https://agupubs.onlinelibrary.wiley.com/doi/abs/10.1029/2020SW002641
[25] P. T. M. Loto'aniu, K. Romich, W. Rowland, S. Codrescu, D. Biesecker, J. Johnson, H. J. Singer, A. Szabo, and M. Stevens, "Validation of the DSCOVR spacecraft mission space weather Solar wind products," *Space Weather*, vol. 20, no. 10, p. e2022SW003085, 2022, e2022SW003085 2022SW003085. [Online]. Available: https://agupubs.onlinelibrary.wiley.com/doi/abs/10.1029/2022SW003085
[26] E. I. Tanskanen, "A comprehensive high-throughput analysis of substorms observed by image magnetometer network: Years 1993–2003 examined," *Journal of Geophysical Research: Space Physics*, vol. 114, no. A5, 2009. [Online]. Available: https://agupubs.onlinelibrary.wiley.com/doi/abs/10.1029/2008JA013682
[27] Y. Wei, B. Zhao, G. Li, and W. Wan, "Electric field penetration into earth's ionosphere: a brief review for 2000–2013," *Science Bulletin*, vol. 60, no. 8, pp. 748–761, 2015. [Online]. Available: https://www.sciencedirect.com/science/article/pii/S2095927316304376
[28] G. Li, B. Ning, Y. Otsuka, M. A. Abdu, P. Abadi, Z. Liu, L. Spogli, and W. Wan, "Challenges to equatorial plasma bubble and ionospheric scintillation short-term forecasting and future aspects in east and southeast Asia," *Surveys in Geophysics*, vol. 42, no. 1, pp. 201–238, 2021. [Online]. Available: https://doi.org/10.1007/s10712-020-09613-5
[29] M. Abdu, "Major phenomena of the equatorial ionosphere-thermosphere system under disturbed conditions," *Journal of Atmospheric and Solar-Terrestrial Physics*, vol. 59, no. 13, pp. 1505–1519, 1997, the Ninth International Symposium on Equatorial Aeronomy. [Online]. Available: https://www.sciencedirect.com/science/article/pii/S1364682696001526
[30] M. A. Abdu, E. A. Kherani, I. S. Batista, and J. H. A. Sobral, "Equatorial evening prereversal vertical drift and spread f suppression by disturbance penetration electric fields," *Geophysical Research Letters*, vol. 36, no. 19, 2009. [Online]. Available: https://agupubs.onlinelibrary.wiley.com/doi/abs/10.1029/2009GL039919
[31] L. Spogli, C. Cesaroni, D. Di Mauro, M. Pezzopane, L. Alfonsi, E. Musicò, G. Povero, M. Pini, F. Dovis, R. Romero, N. Linty, P. Abadi, F. Nuraeni, A. Husin, M. Le Huy, T. T. Lan, T. V. La, V. G. Pillat, and N. Floury, "Formation of ionospheric irregularities over southeast Asia during the 2015 St. Patrick's Day storm," *Journal of Geophysical Research: Space Physics*, vol. 121, no. 12, pp. 12,211–12,233, 2016. [Online]. Available: https://agupubs.onlinelibrary.wiley.com/doi/abs/10.1002/2016JA023222
[32] L. Alfonsi, P. J. Cilliers, V. Romano, I. Hunstad, E. Correia, N. Linty, F. Dovis, O. Terzo, P. Ruiu, J. Ward, and P. Riley, "First observations of GNSS ionospheric scintillations from DemoGRAPE project," *Space Weather*, vol. 14, no. 10, pp. 704–709, 2016. [Online]. Available: https://agupubs.onlinelibrary.wiley.com/doi/abs/10.1002/2016SW001488
[33] X. Pi, A. J. Mannucci, U. J. Lindqwister, and C. M. Ho, "Monitoring of global ionospheric irregularities using the worldwide GPS network," *Geophysical Research Letters*, vol. 24, no. 18, pp. 2283–2286, 1997. [Online]. Available: https://agupubs.onlinelibrary.wiley.com/doi/abs/10.1029/97GL02273
[34] C. Li, C. M. Hancock, N. A. S. Hamm, S. V. Veettil, and C. You, "Analysis of the relationship between scintillation parameters, multipath and ROTI," *Sensors*, vol. 20, no. 10, 2020. [Online]. Available: https://www.mdpi.com/1424-8220/20/10/2877